Phase Transition of $C_5H_5NHSbBr_4$ Having a Hypervalent Bond: A ^2H NMR and X-Ray Diffraction Study *

[Phase Transition of $C_5H_5NHSbBr_4$]

K. Yamada [a], T. Ohtani [a], S. Shirakawa [a], H. Ohki [a], T. Okuda [a], T. Kamiyama [b], and K. Oikawa [b]

[a] Department of Chemistry, Faculty of Science, Hiroshima University, Kagamiyana 1–3, Higashi-Hiroshima 739, Japan
[b] Institute of Materials Science, University of Tsukuba, Tsukuba 305, Japan

Z. Naturforsch. **51a**, 739–744 (1996); received October 11, 1995

The second order phase transition at 253 K of pyridinium tetrabromoantimonate(III), $C_5H_5NHSbBr_4$, has been characterized by means of X-ray diffraction and ^2H NMR. As was suggested from the ^{81}Br NQR spectra, the Rietveld refinements of the X-ray diffraction patterns at 297 K and 116 K confirm the structural change of the anion from $SbBr_4^-$ to $SbBr_3 \cdot Br^-$. The line shape analysis of the ^2H NMR using the deuterated analog revealed that the librational amplitude of the pyridinium ring about the axis normal to the plane increased with temperature and its rms amplitude reaching ca. 25° at T_c. The librational motion may induce the phase transition breaking the hydrogen bonds of the type N–H $\cdots$ Br. However, nearest-neighbor $2\pi/6$ jump or reorientation such as seen in benzene were not observed even at 350 K.

Key words: ^2H NMR, ^{81}Br NQR, Rietveld analysis, Phase transition, Hypervalent bond.

Introduction

In previous papers, we have reported characteristic phase transitions of $C_5H_5NHSbCl_4$ and $C_5H_5NHSbBr_4$ by means of ^{35}Cl and ^{81}Br NQR spectroscopy [1, 2]. In the chloride, two polymorphs (α and β phases) were found at room temperaure depending upon the preparation condition and thermal treatment. The ^{35}Cl NQR spectrum for the β phase (high temperature) suggested that the $SbCl_4^-$ anion has a two-fold symmetry axis, whereas that of the α phase suggested that the anion structure can be described as $SbCl_3 \cdot Cl^-$. On the other hand, as Fig. 1 shows, a dramatic second order phase transition was found for the bromide analog at T_c, below which an extremely large splitting of the ^{81}Br NQR, assigned to the *axial* Br atoms was observed. This extremely large splitting of the NQR below T_c suggests a deformation of the *axial* hypervalent bond with decreasing temperature, i.e., Br–Sb–Br $\rightarrow$ Br–Sb $\cdots$ Br^-. The bond order of the *axial* Br atom, estimated from the NQR frequency, is nearly one-half that of the *equatorial* Br atom. Furthermore, it is interesting to note that the

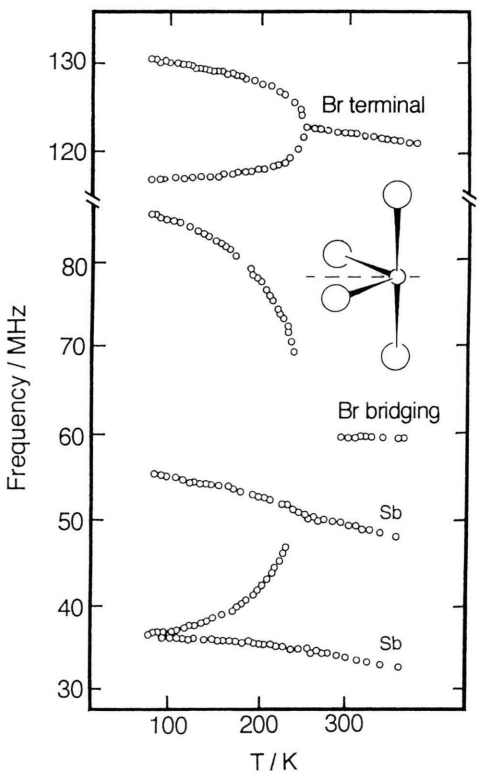

Fig. 1. Temperature dependence of the ^{81}Br and ^{121}Sb NQR frequencies for $C_5H_5NHSbBr_4$ [2].

* Presented at the XIIIth International Symposium on Nuclear Quadrupole Interactions, Providence, Rhode Island, USA, July 23–28, 1995.

Reprint requests to Dr. K. Yamada.

0932-0784 / 96 / 0500-0739 $ 06.00 © – Verlag der Zeitschrift für Naturforschung, D-72072 Tübingen

average of the two NQR frequencies at the *axial* positions remains nearly constant even below T_c despite the extremely large splitting. This type of deformation of the bond is a common feature for hypervalent elements having inert s-electron lone pairs.

In this paper we have investigated the mechanism of the phase transition of the title compound by means of the Rietveld analyses of the X-ray data and ^{2}H NMR spectroscopy. We discuss the dynamic effect of the pyridinium cation on the phase transition, considering the hypervalent nature of the *trans* Br–Sb–Br bond.

Experimental

Pyridinium tetrabromoantimonate(III) was prepared by crystallization from an acidic solution in which equimolar amounts of $SbBr_3$ and pyridinium bromide were dissolved. The salt was washed with ethanol and dried *in vacuo*. The deuterated analog, $C_5D_5NHSbBr_4$, was prepared similarly using pyridine-d_5 instead of pyridine.

Powder X-ray diffraction patterns were taken on the Rigaku Rad B-system using Cu Kα radiation. The Rietveld refinement was performed, using a FORTRAN program "RIETAN" developed by Izumi [3]. Crystallographic data and experimental details are summarized in Table 1. ^{2}H NMR spectra were acquired at 6.37 T ($\nu_L = 41.632$ MHz) on a Matec pulsed spectrometer with a homemade sample prove and a temperature controller. The ^{2}H NMR spectrum was obtained by a fourier transformation of the solid echo. A conventional pulse sequence, 90_x-90_y-echo$_x$, was used, in which the typical pulse length was 4 μs and the pulse separation ca. 50 μs. ^{2}H NMR spectra were symmetrically drawn artificially, because quadrature detection was not used in this experiment.

Results and Discussion

Rietveld Analysis of the Powder X-Ray Patterns at 297 K (Phase I) and 116 K (Phase II)

The crystal structure of pyridinium tetrabromoantimonate(III), $C_5H_5NHSbBr_4$, was first determined by DeHaven and Jacobson using a single crystal [4]. According to them, $C_5H_5NHSbBr_4$ belongs to the monoclinic system and the $SbBr_4^-$ anion could be described as linked in edge-sharing octahedra as shown in Figure 2(A). The $SbBr_6$ octahedra distort considerably. The bond distances are listed in Figure 2(B). It should be emphasized that both the nitrogen and antimony atoms are located on the two-fold axis of the monoclinic system. The possible hydrogen bonds between the bridging Br and N–H bond are also shown symmetrically about the two-fold axis. This structure is consistent with the ^{81}Br NQR spectrum at room temperature (Figure 1). Figure 3 shows the final plot of the Rietveld refinements for $C_5H_5NHSbBr_4$ at 297 K (Phase I) and 116 K (Phase II). In the Rietveld refinement of the structure at 297 K, the atomic coordinates of the carbon and nitrogen atoms were fixed to those reported by DeHaven and Jacobson [4]. The powder pattern at 116 K could be indexed as a triclinic system with space group P$\bar{1}$ (No. 2). The crystal

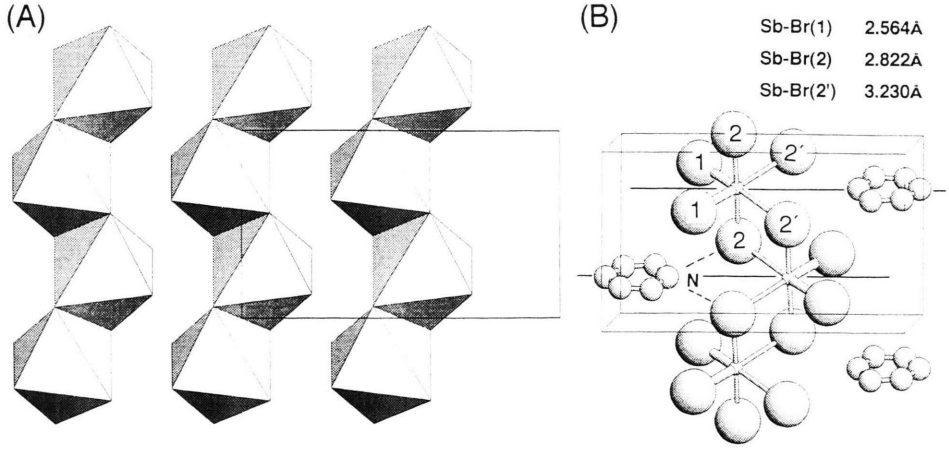

Fig. 2. Crystal structure of $C_5H_5NHSbBr_4$ (room temperature phase). (a) Edge sharing $SbBr_6$ octahedra along the crystal *c*-axis. (b) Possible hydrogen bonds between N–H and bridging Br atoms.

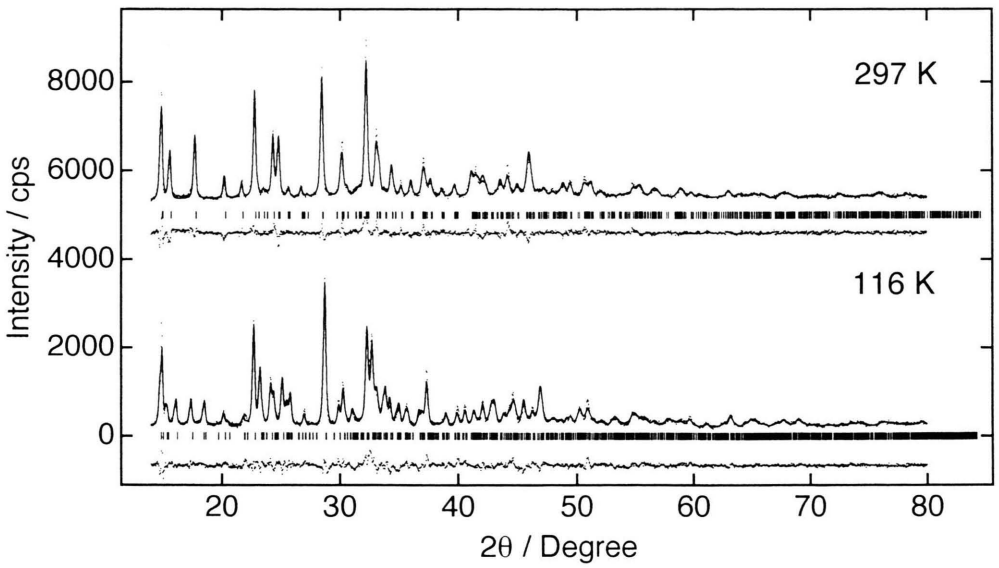

Fig. 3. Final plot of the Rietveld analysis for $C_5H_5NHSbBr_4$ at 297 K and 116 K. Solid lines and dots are calculated and observed patterns, respectively. The differences between them are shown at the lower portions.

axes of Phase II are roughly expressed as,

$$\begin{aligned} \boldsymbol{a}' &= 1/2(\boldsymbol{a} + \boldsymbol{b}), \\ \boldsymbol{b}' &= 1/2(\boldsymbol{a} - \boldsymbol{b}), \\ \boldsymbol{c}' &= \boldsymbol{c}, \end{aligned} \tag{1}$$

where $\boldsymbol{a}'$, $\boldsymbol{b}'$, and $\boldsymbol{c}'$ denote low temperature phase. The initial parameters of the atomic coordinates, which were used in the Rietveld refinement for Phase II, were calculated using the equations

$$\begin{aligned} x' &= x - y + 0.5, \\ y' &= x + y - 0.5, \\ z' &= z, \end{aligned} \tag{2}$$

where 0.5 denotes the translation of the origin from (0, 0, 0) to (0, 0.5, 0). Crystallographic data and atomic coordinates for both phases are summarized in Tables 1 and 2. Figure 4 shows the anion structure together with Sb–Br bond lengths. Only the inversion point of the space group C2/c is maintained in Phase II. As was proposed from the ^{81}Br NQR spectra, the anion structure in Phase II can be described more properly as $SbBr_3 \cdot Br^-$, this anion resulting from the deformation of the relatively weak trans Br–Sb–Br bond. The formation of the hydrogen bond of the type $N-H\cdots Br^-$ may stabilize the ionic form. In the Rietveld refinement for Phase II, however, an isoelec-

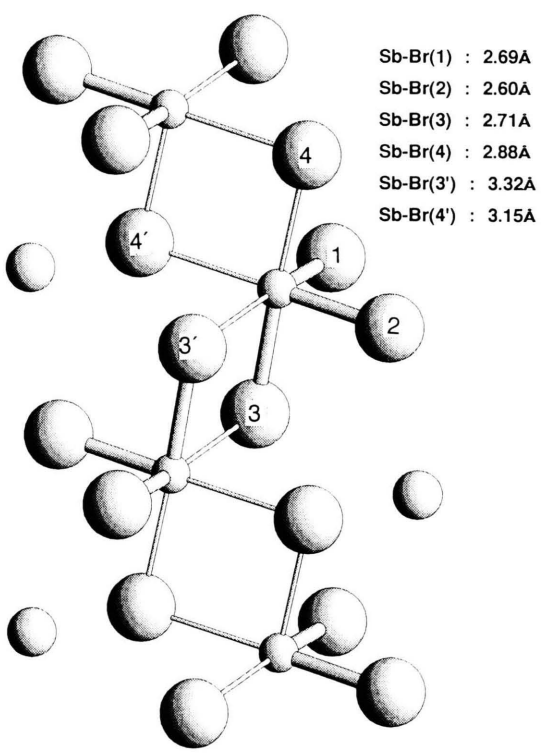

Fig. 4. Anion structure in $C_5H_5NHSbBr_4$ at 116 K. From the bond distances shown in this figure, a deformation of the *trans* Br–Sb–Br bond to $Br-Sb\cdots Br^-$ is clearly seen.

Table 1. Crystal data and experimental details of the Rietveld analyses for $C_5H_5NHSbBr_4$.

Temperature	116 K	297 K [a]
Crystal system	Triclinic	Monoclinic
Space group	$P\bar{1}$ (No. 2)	C2/c (No. 15-2)
Lattice constant	$a=8.674(1)$ Å	$a=11.825(2)$ Å
	$b=8.797(1)$ Å	$b=13.048(2)$ Å
	$c=7.609(1)$ Å	$c=7.698(1)$ Å
	$\alpha=89.96(2)°$	
	$\beta=95.07(2)°$	$\beta=93.87(2)°$
	$\gamma=95.06(2)°$	
z	2	4
d_{cal}	3.005 g/cm^3	2.922 g/cm^3
Number of parameters	50	31
2θ range	14°–80°	14°–80°
Step width	0.04°	0.04°
R_F, R_p [b]	0.012, 0.058	0.019, 0.056
DS, RS, SS [c]	1.0°, 0.3 mm, 1.0°	1.0, 0.3 mm, 1.0°

[a] Single crystal data, $a=11.824(6)$, $b=13.040(5)$, $c=7.703(4)$ Å and $\beta=93.89°$.
[b] $R_p=\sum|y_i(\text{obs})-y_i(\text{cal})|/\sum y_i(\text{obs})$, where $y_i(\text{obs})$ and $y_i(\text{cal})$ are the observed and calculated intensity at the ith step.
$R_F=\sum(\sqrt{I_K(\text{obs})}-\sqrt{I_K(\text{cal})})/\sum\sqrt{I_K(\text{obs})}$, where I_K is the intensity assigned to the Kth Bragg reflection.
[c] Divergence slit, receiving slit, and scatter slit.

Table 2. Positional and thermal parameters of $C_5H_5NHSbBr_4$ at 297 K (Phase I) and 116 K (Phase II).

Tem.	Atom	x	y	z	B_{ISO}/Å
297 K [a]	Sb	0.0	0.0846(8)	0.25	2.2(4)
	Br(1)	−0.1348(8)	0.2222(8)	0.3743(16)	2.5(4)
	Br(2)	0.1374(7)	0.0950(8)	0.5583(10)	3.0(4)
	C(1)	−0.094	0.362	0.807	12.7(17)
	C(2)	−0.089	0.465	0.799	12.7(17)
	C(3)	0.0	0.519	0.75	12.7(17)
	N	0.0	0.316	0.75	12.7(17)
116 K	Sb	0.585(1)	0.410(1)	0.745(1)	0.7(3)
	Br(1)	0.864(1)	0.421(1)	0.614(1)	1.0(4)
	Br(2)	0.613(1)	0.142(1)	0.884(2)	2.3(5)
	Br(3)	0.728(1)	0.540(1)	0.047(1)	0.8(5)
	Br(4)	0.456(1)	0.266(1)	0.418(2)	2.2(6)
	C_5H_5NH [b]	−0.152(5)	0.196(11)	0.296(5)	

[a] Positional parameters of pyridinium cation were not refined.
[b] Isoelectronic dummy atom Tc with anisotropic thermal parameter was used in the refinement.

tronic dummy atom having a large anisotropic thermal parameter was used instead of the pyridinium. We are now preparing to obtain neutron diffraction data (TOF) for both phases in order to get more information on the pyridinium cation below and above T_c. More precise atomic coordinates and the possibility that there is a disordered structure, will be reported.

Temperature Dependence of the ^2H NMR Line Shape

If the molecular motion is slower than 10^3/s or faster than 10^7/s, the line shape ^2H NMR can be simulated easily using e^2Qq_{zz}/h and η considering a broadening factor. In the latter fast limit case, the motionally averaged efg tensor having $\boldsymbol{q}'_{ij}(i,j=x,y,$ and $z)$ components is expressed as a sum of the different orientation with weighted by the equilibrium distribution,

$$\boldsymbol{q}'_{ij}=\sum \boldsymbol{P}(k)\,\boldsymbol{q}_{ij}(k), \tag{3}$$

where $\boldsymbol{P}(k)$ and $\boldsymbol{q}_{ij}(k)$ are the occupation probability and the tensor component of the electric field gradient at the kth site, respectively. The resultant $\boldsymbol{q}'_{ij}$ is then diagonalized and the orientation of the new principal axis system is obtained.

The components of the quadrupole coupling constant (e^2Qq_{ii}/h) and asymmetry parameter (η) can be estimated from the observed spectrum using the following equations,

$$\begin{aligned}
\Delta\nu_1 &= (3/4)|e^2Qq_{zz}/h|(1-\eta)\\
&= (3/2)|e^2Qq_{xx}/h|,\\
\Delta\nu_2 &= (3/4)|e^2Qq_{zz}/h|\cdot(1+\eta)\\
&= (3/2)|e^2Qq_{yy}/h|,\\
\Delta\nu_3 &= (3/2)|e^2Qq_{zz}/h|,\quad (3/2)|\ldots|,
\end{aligned} \tag{4}$$

and

$$\eta=|(e^2Qq_{yy}-e^2Qq_{xx})/e^2Qq_{zz}|, \tag{5}$$

where $\Delta\nu_1$, $\Delta\nu_2$, and $\Delta\nu_3$ are defined in Figure 5. As Fig. 5 shows, a typical powder pattern having an axially symmetric quadrupole coupling constant was observed at 77 K. With increasing temperature the powder pattern changes gradually; the temperature dependence of the e^2Qq_{ii}/h ($i=x$, y, and z) and η are plotted in Figure 6. Although the z and x components decrease continuously, the y component remains constant in the whole temperature range studied. The corresponding motional mode may involve two site jumps or librational motion about the axis normal to the plane. Figure 7 shows the potential wells for these two models together with the possible hydrogen bonds. First is a two-site jump model between potential wells separated by $\pm\theta$. Second is an uniaxial libration with root mean-square (rms) amplitude defined by θ. Both models yield the same result, and the mo-

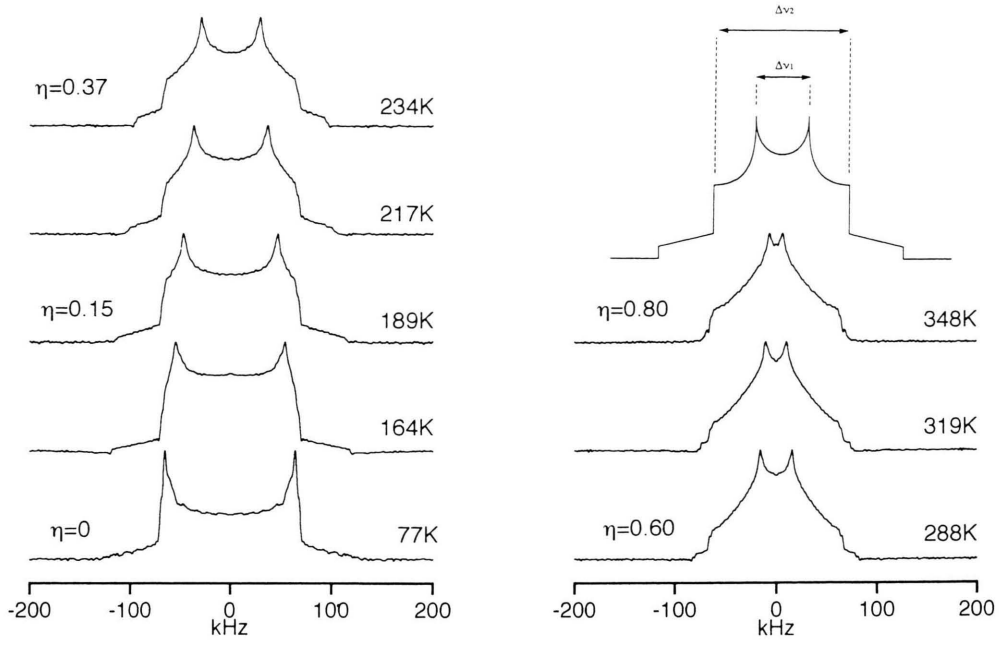

Fig. 5. ^2H NMR spectra for $C_5H_5NHSbBr_4$ in the temperature range from 77 K and 348 K.

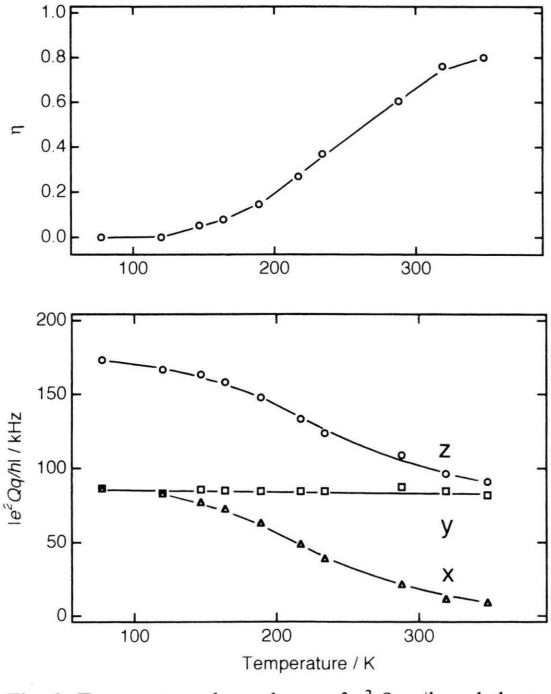

Fig. 6. Temperature dependence of $e^2 Q q_{ii}/h$ and the asymmetry parameter.

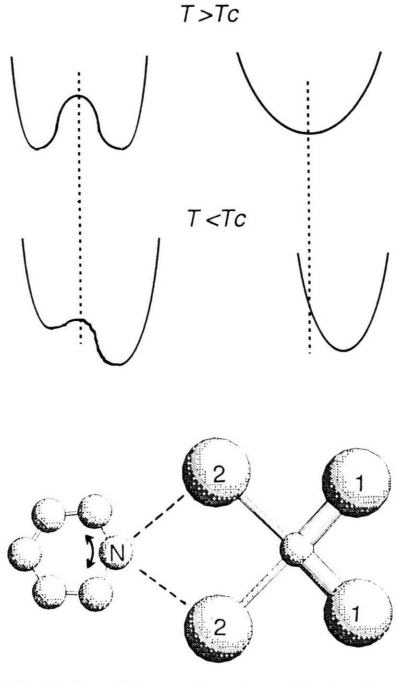

Fig. 7. Possible motional models for the pyridinium ion and the corresponding potential wells below and above T_c.

tionally averaged efg tensor is described by the equations

$$\begin{aligned} q'_{xx} &= q_{xx} \cdot \cos^2\theta + q_{zz} \cdot \sin^2\theta \\ &= (1/2) \cdot q_{zz} \cdot (-3\sin^2\theta + 1), \\ q'_{yy} &= q_{yy} = -(1/2) \cdot q_{zz}, \\ q'_{zz} &= q_{xx} \cdot \sin^2\theta + q_{zz} \cdot \cos^2\theta \\ &= (1/2) \cdot q_{zz} \cdot (-3\cos^2\theta + 1), \end{aligned} \tag{6}$$

and η is expressed as,

$$\eta = 3 \cdot \sin^2\theta/(3\cos^2\theta - 1), \quad \theta < 35.2^\circ. \tag{7}$$

Using (7), the estimated θ is plotted against temperature in Figure 8. No anomalous behavior was observed at T_c. In the case of the two-site jump model, a disorder of the pyridinium ring should be found above T_c. From the structural data and the temperature dependence of the ^2H NMR spectra, the second model is considered to be better, for the following three reasons. First, a disorder of the pyridinium ion was not confirmed in the diffraction experiment [4]. Second, all observed spectra could be simulated as a first limit model. Third, the θ values increased continuously and no anomalous behavior was observed at T_c. Figure 8 plots θ against temperature; the θ values reach ca. 30° at 288 K. However, nearest-neighbor jumps or reorientation about the axis normal to the molecular plane such as observed in the pyridinium cation [5], the cyclopentadienyl group [6], and the benzene molecule [7] was not observed even at 350 K. As the result of this motion, interionic interactions such as hydrogen bonds are averaged over several different directions, and a symmetric *trans* Br–Sb–Br bond appears above T_c.

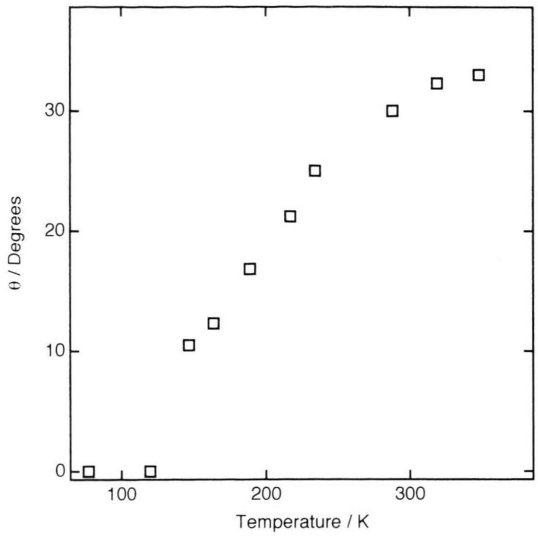

Fig. 8. Rms amplitudes of the librational oscillation versus temperature.

Conclusions

The characteristic phase transition of $C_5H_5NHSbBr_4$ was studied by Rietveld analysis and ^2H NMR experiments. The Rietveld analysis of the XRD pattern at 116 K confirmed the deformation of the anion from $SbBr_4^-$ to $SbBr_3 \cdot Br^-$. The deformation of the anion was strongly affected by the librational motion of the pyridinium cation because the hydrogen bond ($N-H\cdots Br^-$) stabilizes the asymmetric *trans* $Br-Sb\cdots Br^-$ bond.

[1] T. Okuda, Y. Aihara, N. Tanaka, K. Yamada, and S. Ichiba, J. Chem. Soc. Dalton Trans. **1989,** p. 631.
[2] T. Okuda, K. Yamada, H. Ishihara, M. Hiura, S. Gima, and H. Negita, Chem. Soc. Chem. Commun. **1981,** p 979.
[3] F. Izumi, The Rietveld method, Edited by R. A. Young, Oxford University Press, 1993, p. 236.
[4] P. W. DeHaven and R. A. Jacobson, Cryst. Struct. Comm. **5,** 31 (1976).
[5] J. A. Ripmeester, J. Chem. Phys. **85,** 2, 747 (1986).
[6] A. E. Aloev, K. D. Harris, and F. Guillaume, J. Phys. Chem. **99,** 1156 (1995).
[7] M. A. Altbach, Y. Hiyama, R. J. Wittebort, and L. G. Butler, Inorg. Chem. **29,** 741 (1990).